THERMAL OPTIMIZATION AND EXPERIMENTAL DEMONSTRATION OF A SILICON CARBIDE, HALF-BRIDGE POWER MODULE

Gilberto Moreno, Joshua Major, Faisal Khan, and Sreekant Narumanchi
National Renewable Energy Laboratory
15013 Denver West Pkwy
Golden, Colorado 80401
Ph: 303-275-4450
Email: Gilbert.Moreno@nrel.gov

Abstract
This paper describes modeling and experimental work to design and demonstrate a silicon carbide (SiC), single-side-cooled power module. Two SiC metal-oxide-semiconductor field-effect transistors (MOSFET) were used for each switch position and packaged on a metalized ceramic substrate. Thermal modeling was first conducted to optimize the module packaging to minimize junction-to-fluid thermal resistance and device temperature variations. This procedure identified the optimal device placement and baseplate thickness to maximize thermal performance. A heat exchanger – incorporating impinging jets of water-ethylene glycol - was designed to cool the module's baseplate to minimize thermal resistance and pumping power. The heat exchanger used relatively low fluid velocities (<1.5 m/s) to minimize erosion-corrosion effects and relatively large fluid channel sizes (≥1 mm) to prevent clogging. The power module concept was fabricated, and experiments were conducted to measure its thermal performance. Direct current was used to power the module devices, and junction temperatures were measured via device temperature-sensitive parameters. The experimental results were found to be in good agreement with model predictions (within 2%) and yielded junction-to-fluid thermal resistance values as low as about 15 $mm^2 \cdot K/W$ at relatively low pumping power values. The results demonstrate the improved performance associated with jet impingement cooling and represent an improvement over existing channel-flow-type cold plates, which can enable improvements to power density and reliability.

Key words
Thermal management, power electronics, MOSFET power module, wide-bandgap devices, reliability

I. Introduction
Designing an efficient thermal management system to provide low thermal resistance and uniform device temperatures is essential for reliable power electronics operation. Temperature-related stresses are known to be a leading cause of failure for power electronics components [1], [2], [3]. Mitigating these thermal-related failures requires high-fidelity modeling to design a thermal management system to manage steady-state and transient operating conditions.

The majority of automotive power modules are cooled using water-ethylene glycol (WEG) coolant and use channel-flow-type cold plates [4], [5], [6]. Pin-fin- and folded-fin-type fin structures are commonly used surface enhancement features found in automotive power module cold plates that provide relatively good thermal performance. The folded-fin-style structures also provide an economical thermal management solution. In all automotive cases, WEG coolant is pumped across the fins (i.e., fluid flow parallel to the heated cold plate surface) to extract heat.

Jet impingement cooling impinges fluid jet(s) (i.e., fluid flow normal to the heated surface) onto the heated surface to dissipate heat. The thin boundary layers at the impingement zone provide high heat transfer coefficients [7], and the jets can be positioned to provide cooling directly at the heat source. Osman et al. [8], [9] designed a WEG jet impingement cooling system for an automotive power module. The jet-based cooling system used circular jets combined with pin-fin structures to provide relatively high heat transfer coefficients of about 40,000 $W/m^2 \cdot K$. Jet impingement-based cooling strategies for power electronics have also been reviewed by [3], [10].

This paper summarizes the modeling and experimental validation of a jet impingement-cooled, silicon carbide (SiC) module. The concept uses a 3D-printed fluid manifold to provide cooling (via slot jets) to four SiC devices that make up the half-bridge module. Modeling was first used to optimize certain package and cold plate dimensions to improve reliability by reducing thermal resistance, improving device temperature uniformity, and minimizing pumping power. The final design was then fabricated and used for an experimental demonstration. Experiments were then conducted to measure the junction-to-fluid thermal resistance and pumping power at different conditions to validate model predictions. The SiC device's electrical parameters were used to measure the junction temperatures, which were then used to compute thermal resistance values.

II. Methods

This section describes the approach used to design a single-side-cooled, SiC half-bridge module consisting of two 650 V SiC metal-oxide-semiconductor field-effect transistors (MOSFET) per switch position. The devices were soldered to an aluminum nitride ceramic substrate. The ceramic substrate was then soldered to a copper baseplate that was directly cooled with WEG. SAC305 was the solder used for the device and substrate bonding. The goal was to design a cooling system that meets automotive requirements intended to prevent clogging (fluid channel size ≥1 mm) and minimizes erosion-corrosion effects (limit average velocities to <2 m/s).

The modeling approach used to design the package is described first, followed by a description of the experimental apparatus and procedures. WEG coolant (50/50 mixture by volume) entering the module cold plate at 65°C and 3.3 L/min (55.5 cm^3/s) were the operating conditions used to design the system. The WEG directly cooled the module's baseplate (i.e., no thermal interface material) using single-phase heat transfer. The fabrication and experimental demonstration of the module and cooling system are the focus of this paper.

A. Modeling Design

The finite element method and computational fluid dynamics (CFD) were used to design the SiC package and its cold plate. Fig. 1 summarizes the design process. First, a small, device-scale CFD model was used to design the fin and slot jet dimensions. This process provided the heat transfer coefficient boundary condition that was used in a finite element model of the entire module. The model was then used to optimize the device placement and copper baseplate thickness to minimize thermal resistance and device temperature variation. Finally, CFD modeling was used to design the fluid manifold to deliver fluid to the module's four SiC devices. Table 1 provides the material and fluid properties used in the model.

Fig. 2 shows computer-aided design (CAD) drawings of the final power module and cooling system design. The final design used eight linear fins that were 0.5 mm wide and 3 mm tall centered directly behind each device. A 1 mm channel spacing between each fin was used to comply with automotive requirements intended to prevent clogging issues. A 12 mm × 1 mm slot jet was centered directly over the fin areas and generated average jet velocities of about 1.2 m/s. This design achieved a heat transfer coefficient of approximately 37,000 W/m^2·K. Additional details of the design can be found in [11].

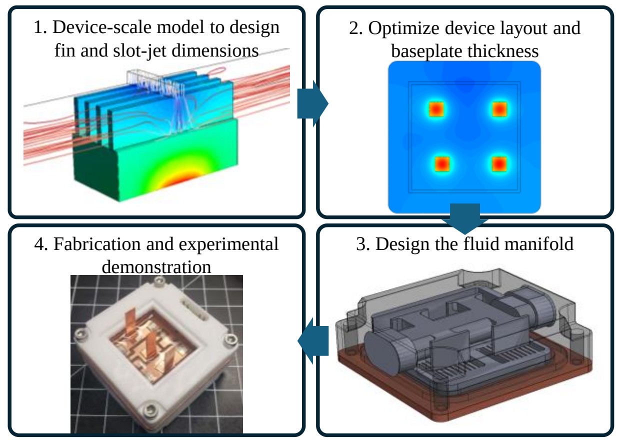

Figure 1. Schematic showing the design and experimental demonstration approach.

Table 1. Material and fluid properties used for the modeling work.

Material/ Fluid	Thermal Conductivity [W/m·K]	Density [kg/m^3]	Specific Heat [J/kg·K]	Viscosity [Pa·s]
SiC [12]	118 (at 150°C)	-	-	-
Copper	390	-	-	-
Aluminum nitride [13]	170	-	-	-
Solder	50	-	-	-
WEG [14]	0.42	1,038	3,494	1.26×10^{-3}

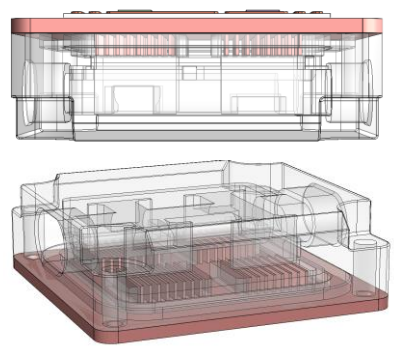

Figure 2. CAD drawing of the final power module and cold plate design. The fluid manifold is shown transparent.

B. Experimetal Apparatus and Procedures

The SiC module was then fabricated according to the modeling results (Fig. 3). The finned copper baseplate was fabricated using an electrical discharge machining method. The fluid manifold was additively manufactured (stereolithography) out of Rigid 10K [15] to allow for fabrication of the intricate, internal fluid flow channels. Fig. 4 shows the fluid manifold and fin structures. Digital microscope measurements reveal good agreement between the fabricated parts and the design requirements. Two pressure ports were provided in the fluid manifold to allow for pressure drop measurements.

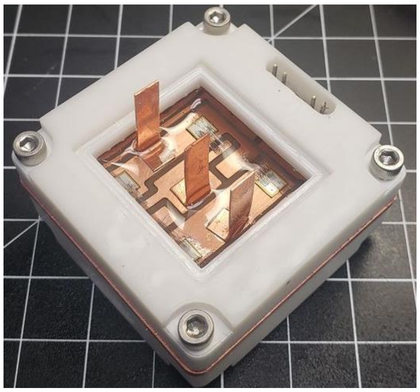

Figure 3. The assembled SiC module and cold plate.

The module and cold plate assembly was then piped into a WEG test bench for the experiments. The WEG was circulated through the module cold plates at flow rates of 1.7 L/min (28.2 cm^3/s), 2.5 L/min (41.7 cm^3/s), and 3.3 L/min (55.5 cm^3/s) and 65°C inlet temperatures. A Siemens 2400 Power Tester was used to power the devices and measure device temperatures to compute junction-to-fluid thermal resistance values. SiC device temperatures were measured using the MOSFET's internal body diode. Calibration procedures were first conducted from 60°C up to 100°C to obtain the temperature-versus-voltage correlations. Junction-to-fluid thermal resistance values were obtained via the Power Tester following the procedures outlined in the JEDEC 51-1 standard [16]. A schematic of the flow loop is provided in Fig. 5. Experiments were conducted by heating the two SiC devices that make up the high-side switch (i.e., only two devices were powered during the experiments).

C. Uncertainty Analysis

An uncertainty analysis was conducted following the procedures described in [17]. Fluid inlet and outlet thermocouple probes (K-type) were calibrated, resulting in an estimated ±0.1°C uncertainty. Pressure drop measurements were obtained using a Setra Model 230 differential pressure transducer with a 0–13.8 kPa (0–2 psi) measurement range. A Coriolis mass flow meter was used to measure fluid flow rates. The estimated uncertainty of the pressure and flow rate measurements are <2% and <1%, respectively. Obtaining the junction temperatures of the devices requires a temperature extrapolation procedure to eliminate electrical transient effects. The temperature extrapolation process makes it difficult to estimate the thermal resistance uncertainty. Thus, the thermal resistance values provided in figure plots are the average of three measurements, and the error bars correspond to the minimum and maximum measured values. Every test condition was repeated three times.

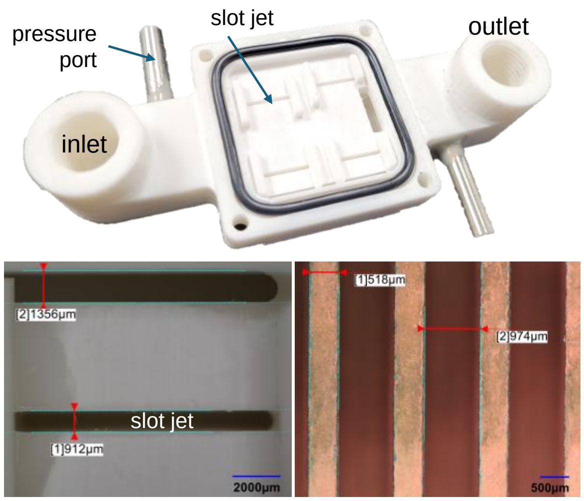

Figure 4. The 3D-printed fluid manifold (top) and digital microscope images of the fluid manifold (bottom left) and copper heat sink fins (bottom right).

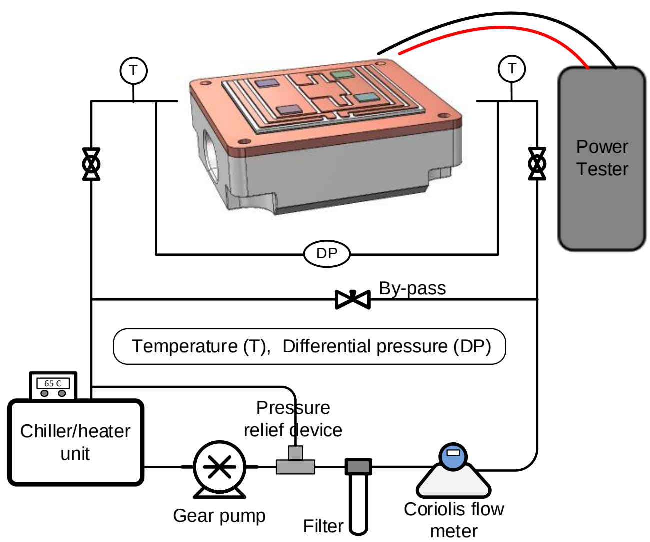

Figure 5. Schematic of the WEG flow loop.

III. Results and Discussion

The CFD modeling and experimental results are provided in this section. The CFD model was modified to replicate the experimental conditions where only the two SiC devices were powered. The experimental results were then provided and compared with model predictions at various conditions.

A. Modeling Results

The CFD model was adjusted to replicate the experimental conditions where only two devices were powered. The model imposed a device heat flux of 170 W/cm^2 on the source side of the SiC MOSFET devices. A mass flow rate inlet boundary condition was imposed at the cold plate inlet using WEG (50/50 mixture by volume) entering at 65°C.

Fig. 6 shows the CFD-computed temperature contours and velocity streamlines for three flow rate cases. Maximum device temperatures of 94.6°C were predicted for the 1.7 L/min flow rate. Device temperature decreases to 92.5°C at the highest flow rate of 3.3 L/min. Additionally, the temperatures of the two paralleled devices are predicted to be within 1°C of each other. Similar temperatures are ideal because it allows for balanced current sharing between the paralleled devices, thus improving reliability. Local velocities of up to 2.5 m/s are computed, but average channel velocities are maintained below 1.5 m/s to minimize erosion-corrosion effects to improve durability.

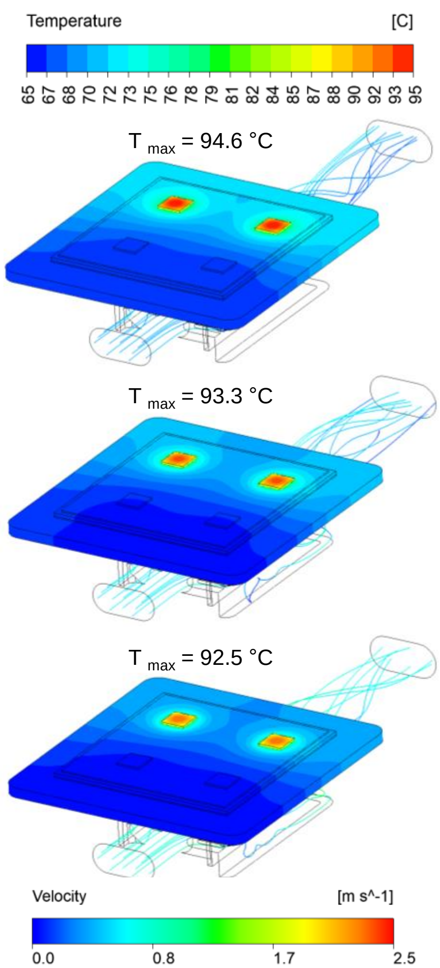

Figure 6. CFD-computed temperature contours and velocity streamlines for 1.7 L/min (top), 2.5 L/min (middle), and 3.3 L/min (bottom) flow rate conditions.

B. Experimental Results

The Power Tester was used to measure the junction-to-fluid thermal resistance. Ninety amps of current was run across the two parallel SiC devices that make up the high-side switch, resulting in approximately 170 W/cm^2 device heat flux dissipation. WEG coolant entering at 65°C was circulated through the module cold plate at various flow rates to provide cooling. A picture of the module piped into the WEG loop and electrically connected to the Power Tester is shown in Fig. 7.

Pressure drop (inlet to outlet) versus flow rate values from experiments and model predictions are provided in Fig. 8. The measured pressure drop values are higher (as much as 17% higher at 1.7 L/min) than model-predicted values. This is likely due to the slightly smaller channel sizes of the fabricated part compared to the model. For example, the slot width and fin channel gap were 0.92 mm and 0.97 mm, respectively, whereas the model assumed a 1 mm value for both. Additionally, the 3D fabrication produced a rough surface texture on the fluid manifold, which is not included in the model and likely also contributes to the higher measured pressure drop values. Better agreement of 5% deviation between model predictions and experiments is observed at the highest flow rate of 3.3 L/min. Overall, the pressure versus flow rate trend is very similar for both.

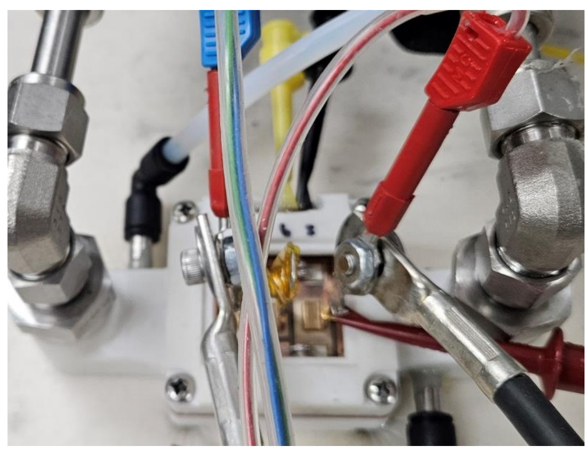

Figure 7. The module with fluid and electrical connections.

Junction-to-fluid specific thermal resistance versus flow rate values are provided in Fig. 9. The specific thermal resistance (R''_{th}) is computed per Eq. 1:

$$R''_{th} = \left(T_{device} - T_{fluid}\right) / \, Heat\ flux \qquad (1)$$

where T_{device} is the temperature of the device, T_{fluid} is the fluid inlet temperature, and *Heat flux* is the device heat flux.

Thermal resistance values computed using the maximum and average device temperatures (T_{device}) are provided for the model predictions. The top-side area-averaged temperature for the two SiC devices was used to compute the model's average thermal resistance values (see Fig. 9). The average temperatures are more representative of how the devices' temperatures are measured and thus a better comparison to the experimentally measured values.

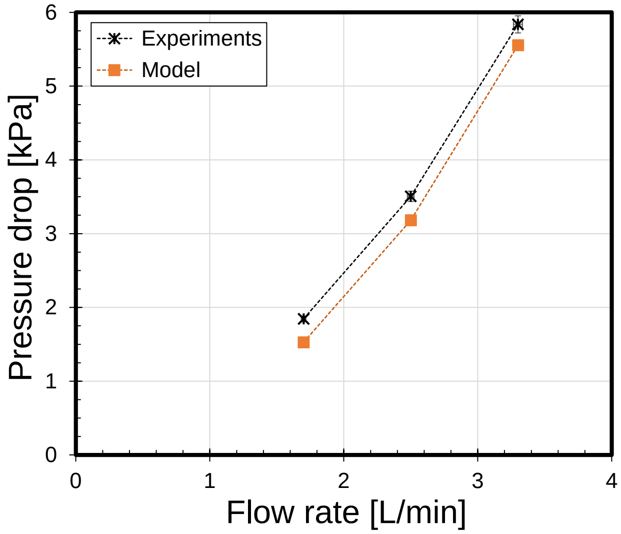

Figure 8. Measured and predicted pressure drop versus flow rate curves.

A model calibration was conducted to match model-predicted thermal resistance values to the measured values for the 2.5 L/min flow rate condition. This calibration procedure adjusted the solder thickness values for both the die- and substrate-attach interfaces so that the model accurately predicted the thermal resistance at one flow rate condition. Die- and substrate-attach solder thickness values of 0.08 mm and 0.3 mm, respectively, were found to provide a good match between the model and experiments for the 2.5 L/min case. These solder thickness values are consistent with typical power module packaging designs and were kept the same for the other flow rate conditions. No other parameters were modified for this calibration.

Good agreement is observed between the measured and model-predicted average thermal resistance values for all three flow rate cases. The maximum deviation between model and experiments was less than 2% for the highest flow rate condition. Specific thermal resistance values as low as about 15 $mm^2 \cdot K/W$ were measured for the 3.3 L/min case at a reasonable 5.8 kPa (0.85 psi) pressure drop. The use of an aluminum nitride ceramic substrate, combined with the relatively high heat transfer coefficients associated with jet impingement, provided a relatively high thermal performance for the SiC module. For comparison, the 2015 BMW i3 has a specific thermal resistance of about 49 $mm^2 \cdot K/W$, while a SiC-based power module (CREE WAB400M12BM3) cooled using a Wieland cold plate (CP3009) has a specific thermal resistance of about 25 $mm^2 \cdot K/W$ [18].

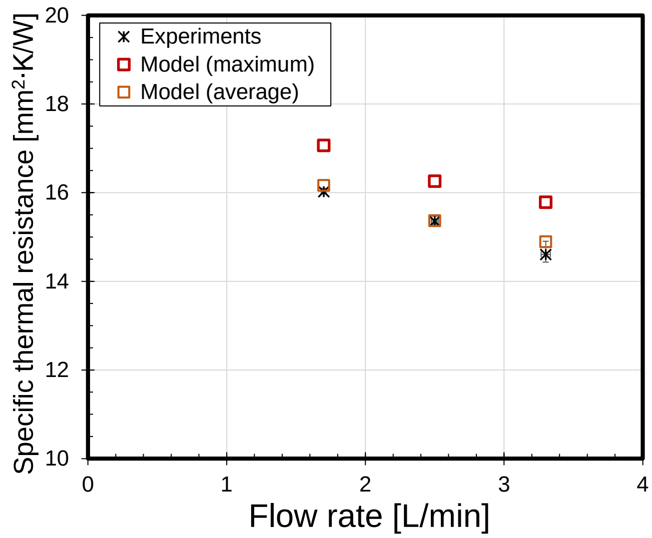

Figure 9. Measured and predicted specific thermal resistance versus flow rate curves.

III. Conclusions

A WEG jet impingement-based cooling system was designed for a SiC half-bridge power module. Modeling work was first conducted to optimize the key module features. The final design was then fabricated at the National Renewable Energy Laboratory and used for an experimental demonstration. Key findings from this study are listed below:

- There was good agreement between model predictions and the experimentally measured values for both the pressure drop and junction-to-fluid thermal resistance values at various flow rates.
- The combination of low package resistance (aluminum nitride ceramic) and high heat transfer coefficients from jet impingement provides a relatively low junction-to-fluid thermal resistance. Specific thermal resistance values as low as about 15 $mm^2 \cdot K/W$ were measured for the highest flow rate condition of 3.3 L/min at a reasonable 5.8 kPa (0.85 psi) pressure drop.
- The low total thermal resistance combined with the relatively uniform device temperatures (within 1°C) represent an improvement over existing power module performance. This, combined with the use of relatively large fluid channels (≥1 mm) to prevent clogging and low fluid velocities (to minimize erosion-corrosion effects), enable improvements to the module's reliability.

Acknowledgments

This work was authored by the National Renewable Energy Laboratory, operated by Alliance for Sustainable Energy, LLC, for the U.S. Department of Energy under Contract No. DEAC36-08GO28308. The funding was provided by the NREL Laboratory Directed Research and Development Program. The views expressed in the article do not necessarily represent the views of the U.S. Department of Energy or the U.S. Government. The U.S. Government retains and the publisher, by accepting the article for publication, acknowledges that the U.S. Government retains a nonexclusive, paid-up, irrevocable, worldwide license to publish or reproduce the published form of this work, or allow others to do so, for U.S. Government purposes.

References

[1] C. Wang, B. Ji, X. Song, V. Pickert, and W. Cao, "IGBT condition monitoring with system identification methods," in *2014 IEEE Conference and Expo Transportation Electrification Asia-Pacific (ITEC Asia-Pacific)*, Beijing, China: IEEE, Aug. 2014, pp. 1–6. doi: 10.1109/ITEC-AP.2014.6941216.

[2] A. Hanif, Y. Yu, D. DeVoto, and F. Khan, "A Comprehensive Review Toward the State-of-the-Art in Failure and Lifetime Predictions of Power Electronic Devices," *IEEE Trans. Power Electron.*, vol. 34, no. 5, pp. 4729–4746, May 2019, doi: 10.1109/TPEL.2018.2860587.

[3] S. Jones-Jackson, R. Rodriguez, and A. Emadi, "Jet Impingement Cooling in Power Electronics for Electrified Automotive Transportation: Current Status and Future Trends," *IEEE Trans. Power Electron.*, vol. 36, no. 9, pp. 10420–10435, Sep. 2021, doi: 10.1109/TPEL.2021.3059558.

[4] Y. Yang, L. Dorn-Gomba, R. Rodriguez, C. Mak, and A. Emadi, "Automotive Power Module Packaging: Current Status and Future Trends," *IEEE Access*, vol. 8, pp. 160126–160144, 2020, doi: 10.1109/ACCESS.2020.3019775.

[5] J. Broughton, V. Smet, R. R. Tummala, and Y. K. Joshi, "Review of Thermal Packaging Technologies for Automotive Power Electronics for Traction Purposes," *Journal of Electronic Packaging*, vol. 140, no. 4, Aug. 2018, doi: 10.1115/1.4040828.

[6] G. Moreno, S. Narumanchi, X. Feng, P. Anschel, S. Myers, and P. Keller, "Electric-Drive Vehicle Power Electronics Thermal Management: Current Status, Challenges, and Future Directions," *Journal of Electronic Packaging*, vol. 144, no. 1, Mar. 2022, doi: 10.1115/1.4049815.

[7] F. P. Incropera, *Liquid Cooling of Electronic Devices by Single-Phase Convection*. John Wiley & Sons, Inc., 1999.

[8] A. Osman, G. Moreno, S. Myers, S. V. J. Narumanchi, and Y. Joshi, "Single-Phase Jet Impingement Cooling for a Power-Dense Silicon Carbide Power Module," *IEEE Transactions on Components, Packaging and Manufacturing Technology*, vol. 13, pp. 615–627, 2023, doi: 10.1109/TCPMT.2023.3276712.

[9] A. Osman *et al.*, "Automotive Silicon Carbide Power Module Cooling With A Novel Modular Manifold And Embedded Heat Sink," *Journal of Electronic Packaging*, pp. 1–13, Jun. 2023, doi: 10.1115/1.4062869.

[10] C. Klinkhamer, K. L. V. Iyer, M. Etemadi, R. Balachandar, and R. Barron, "Jet Impingement Heat Sinks With Application Toward Power Electronics Cooling: A Review," *IEEE Trans. Compon., Packag. Manufact. Technol.*, vol. 13, no. 6, pp. 765–787, Jun. 2023, doi: 10.1109/TCPMT.2023.3288612.

[11] G. Moreno *et al.*, "Thermal Optimization of a Silicon Carbide, Half-Bridge Power Module," in *ASME InterPACK2022*, Anaheim, CA, Oct. 2022. doi: 10.1115/IPACK2022-97283.

[12] R. Wei *et al.*, "Thermal conductivity of 4H-SiC single crystals," *Journal of Applied Physics*, vol. 113, no. 5, p. 053503, Feb. 2013, doi: 10.1063/1.4790134.

[13] "Curamik Ceramic Substrates - DBC Technology Design Rules.pdf."

[14] K. Alshamani, "Equations for physical properties of automotive coolants," SAE Technical Paper, 2003.

[15] "Rigid 10K Resin," Formlabs. Accessed: Jun. 17, 2024. [Online]. Available: https://formlabs.com/store/materials/rigid-10k-resin/

[16] JEDEC, *Integrated Circuits Thermal Measurement Method - Electrical Test Method (Single Semiconductor Device)*, vol. JEDEC-51-1. 1995. [Online]. Available: https://www.jedec.org/standards-documents/docs/jesd-51-1

[17] R. H. Dieck, *Measurement Uncertainty: Methods and Applications*, 4th ed. Research Triangle Park, NC, USA: ISA, 2007.

[18] G. Moreno and S. Narumanchi, "Dielectric Fluid Cooling of Power Electronics Modules," *IEEE EPS Newsletter*, 2024,https://eps.ieee.org/publications/enews/february-2024.html